Journal of
Water & Climate Change

IWA PUBLISHING

Journal of Water and Climate Change Vol 00 No 0, 1 doi: 10.2166/wcc.2026.312

Compounding heat waves and extreme precipitation in India using event coincidence analysis

Swarnendu Saha [a], Divya Sardana [b,*], Ashish Manoj J. [b,c] and Ankit Agarwal [b,d]

[a] Department of Physical Sciences, Indian Institute of Science Education and Research Kolkata, Kolkata, West Bengal, India
[b] Department of Hydrology, Indian Institute of Technology Roorkee, Roorkee, Uttarakhand, India
[c] Chair of Hydrology, Karlsruhe Institute of Technology, Karlsruhe, Germany
[d] GFZ Helmholtz Centre for Geosciences, Potsdam, Germany
*Corresponding author. E-mail: divya.pd@hy.iitr.ac.in

SS, 0009-0001-3614-532X; DS, 0009-0007-3111-4966

ABSTRACT

The increasing frequency of compound extremes, such as heat waves followed by heavy rainfall, present significant challenges due to their amplified regional impacts. This study quantifies the association between heat waves and heavy rainfall across India from 1951 to 2020, using Event Coincidence Analysis to measure the Precursor Coincidence Rate (PCR) and Trigger Coincidence Rate (TCR). PCR assesses the likelihood of heat waves preceding rainfall, while TCR indicates proportion of rainfall events following heat waves. Results reveal decline in TCR for shorter windows ($\Delta T = 2, 5$) but notable increases (50%) over longer windows ($\Delta T = 7$) in recent period, with approximately 70% of grid points exhibiting this trend. This suggests enhanced atmospheric moisture capacity and delayed convective processes drive rainfall after heat waves. PCR increased consistently across all windows, with 27% of grid points recording a heat wave within seven days before heavy rainfall in recent period, compared to 13% in base period. Seasonal analysis highlights stronger heat wave-rainfall coupling during winter and pre-monsoon, with heightened variability in recent decades. During monsoon, abundant moisture moderates this coupling, though sporadic extreme events persist. These results underscore the importance of understanding seasonal and temporal variations in compound extremes under climate change.

Key words: compound events, event coincidence analysis, heat waves, heavy rainfall, precursor coincidence rate, seasonal coupling, trigger coincidence rate

HIGHLIGHTS

- PCR rises, showing higher rainfall probability within 7 days of heat waves.
- TCR falls for short windows ($\Delta T = 2,5$) but increases 50% at $\Delta T = 7 \rightarrow$ delayed rainfall.
- Heat wave–rainfall links grew from 13% → 27%, tied to higher moisture & convection.
- Stronger pre-monsoon & winter coupling signals intensified climate variability.

GRAPHICAL ABSTRACT

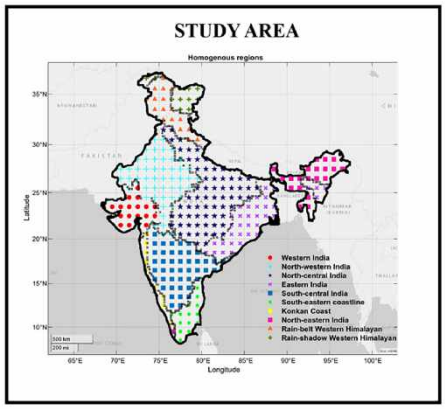

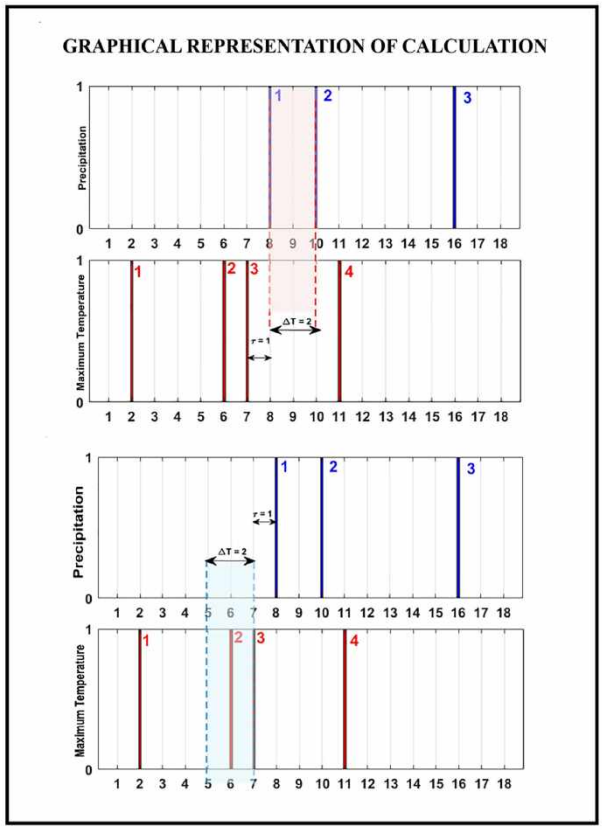

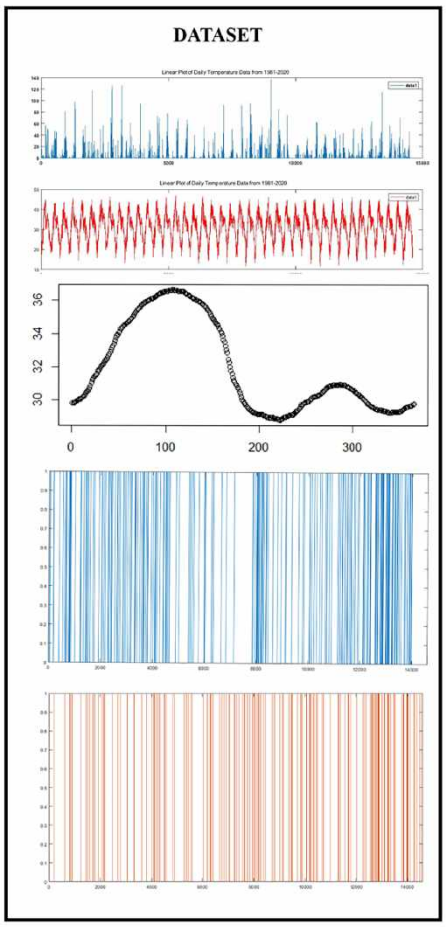

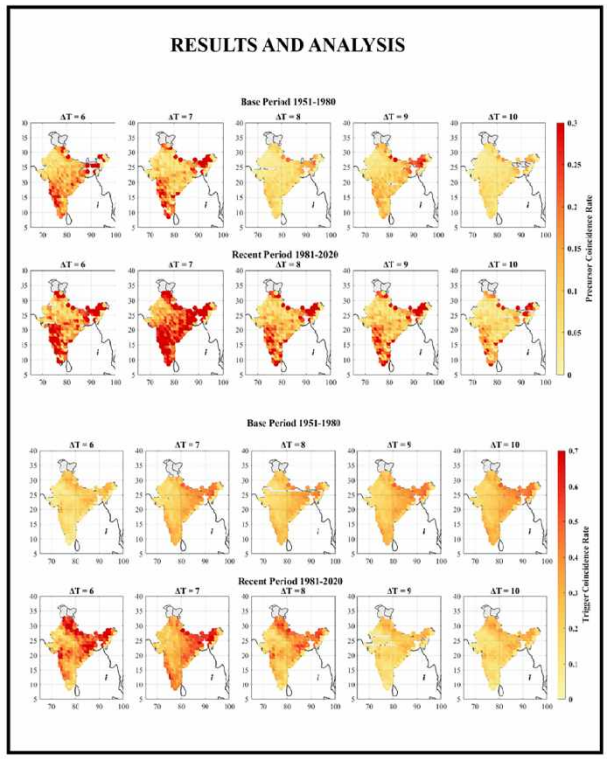

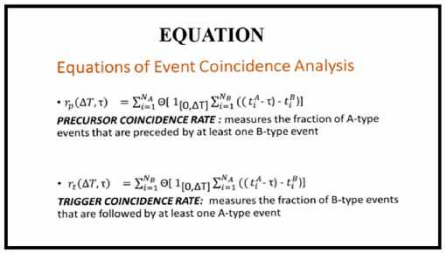

1. INTRODUCTION

Global warming has significantly altered the climate system, intensifying the hydrological cycle through positive radiative feedback (Trenberth *et al.* 2014). This has led to more frequent, intense, and severe extreme weather events, highlighting the growing need for comprehensive risk assessment studies (Wu *et al.* 2023). Globally, heat waves have caused pronounced human fatalities, about 166,000 deaths reported between 1998 and 2017, with approximately 70,000 fatalities during the 2003 European heat wave (Barriopedro *et al.* 2023). Economic losses due to heat waves have been substantial, averaging around US$74 billion annually between 2009 and 2019 (CRED 2020). Rising temperatures enhance the atmosphere's moisture-holding capacity, thereby intensifying heavy rainfall and flooding, as observed across East Asia, North America, and Europe (Trenberth *et al.* 2014; Donat *et al.* 2016). When heat waves and heavy rainfall occur together or in close succession, their compounding effects can greatly amplify impacts – intensifying flooding, disrupting agriculture, and straining infrastructure and health systems. Understanding such compound events has thus become a challenge for climate risk assessment and adaptation planning (Rahmstorf & Coumou 2011; Sauter *et al.* 2023).

To examine these compound event interactions, the Indian subcontinent provides a particularly compelling context, given its diverse climate regimes, high population density and pronounced vulnerability to climate hazards. At the national scale, Guntu & Agarwal (2024)documented a statistically significant increase of approximately 0.61% per year in compound hot-wet events across India, exemplified by hot nights occurring alongside wet days. Complementing this large-scale evidence, recent observational studies have revealed a strong statistical coupling between humid heatwave characteristics and subsequent short-duration extreme precipitation over Indian cities, especially in coastal regions, pointing to an elevated risk of cascading heat stress and flood hazards (Ganguli & Merz 2024). Event-based analyses further demonstrate that extreme rainfall in the Chennai Metropolitan Area is significantly amplified when preceded by intense heatwaves, resulting in increased pluvial flood hazard and population exposure, and underscoring the real-world consequences of compound hot–wet extremes in India (Ganguli *et al.* 2025). Consistent with these findings, several regions across India have experienced closely spaced sequences of humid heatwaves followed by extreme precipitation, with documented impacts on energy demand (Stone *et al.* 2021), forests and agriculture (You *et al.* 2023), human health (Bansal *et al.* 2023), infrastructure (Prein *et al.* 2017; Kotz *et al.* 2022).

On global scales, research has extensively examined the co-occurrence and interaction of multiple climate extremes using observations and climate model simulations (Hao *et al.* 2018; Zscheischler *et al.* 2018, 2020; Agha Kouchak *et al.* 2020). Comprehensive assessments have identified several classes of compound hydro-meteorological extremes, including hot–dry, hot–wet, cold–wet, cold–dry, and compound flood events, all of which pose substantial socio-economic risks (Sedlmeier *et al.* 2018; Li *et al.* 2020; Ridder *et al.* 2020). While hot–dry extremes have been widely studied across multiple regions, including India (Mishra *et al.* 2020; Guntu & Agarwal 2021), growing evidence indicates that hot–wet events – often manifested as precipitation extremes following or coinciding with heatwaves – are increasing in frequency and intensity at the global scale, particularly in densely populated and urban regions (Luo & Lau 2021). Recent studies further demonstrate that such heatwave-preconditioned rainfall events can act as cascading hazards, where antecedent thermal stress modifies atmospheric and land-surface conditions, enhancing the likelihood of short-duration extreme precipitation and pluvial flooding (Wahl *et al.* 2015; Moftakhari *et al.* 2017). These findings underscore the need for methodological frameworks that can explicitly resolve the timing, sequencing, and directionality of heat–precipitation interactions, especially in climate-vulnerable regions such as India.

Numerous existing studies rely on correlation-based metrics or probabilistic dependence frameworks, which primarily quantify the strength of association between temperature and precipitation extremes but do not explicitly resolve event sequencing, timing, or directionality (Siegmund *et al.* 2016). Consequently, lagged or asymmetric interactions that are characteristic of cascading hazards may remain obscured. While univariate approaches have substantially advanced the understanding of heatwaves and heavy rainfall as independent hazards, their joint or consecutive manifestation can amplify impacts well beyond those inferred from single-event analyses, underscoring the need for event-based methods that explicitly track how extremes unfold in time.

Recent studies have applied conditional probability and copula-based frameworks to examine hot–wet extremes in India. For example, Ganguli & Merz (2024) demonstrated statistically significant amplification of short-duration extreme precipitation conditioned on humid heatwave characteristics, particularly in coastal cities. While such approaches provide valuable estimates of risk amplification and tail dependence, they remain agnostic to the temporal ordering of extremes and cannot

directly identify whether heatwaves act as antecedent drivers that precondition the atmosphere or land surface for subsequent rainfall. Similarly, although Event Coincidence Analysis (ECA) has been applied in India to precipitation–soil moisture interactions (Manoj *et al.* 2022), its potential to resolve directional heat–precipitation coupling and associated hazard implications has not yet been explored. As a result, a key research gap persists in distinguishing precursor versus triggering relationships in Indian hot–wet extremes, which is essential for early warning, impact attribution, and adaptation planning.

To address this gap, we provide a first national-scale, grid-level analysis of compound hot-wet extremes across mainland India using ECA. ECA is a statistically rigorous and scale-independent framework designed to quantify the timing, directionality and temporal sequencing between heat waves and extreme rainfall. Unlike probabilistic or copula-based methods – whether parametric or non-parametric – ECA does not estimate dependence in distribution space but instead focuses on the event structure itself. Using two directional indicators, the Precursor Coincidence Rate (PCR) and the Trigger Coincidence Rate (TCR), we explicitly assess whether heatwaves systematically precede extreme rainfall or whether rainfall events tend to follow heat waves within a short time window. Seasonal stratification of these relationships further reveals pre-monsoon and monsoon-specific coupling that are obscured in annual or probability-based analyses.

The rest of the article is structured as follows. Section 2 outlines the study area and data utilized. Section 3 details the methodology used in this study. Section 4 discusses the results of this study, which include the spatio-temporal distribution of PCR, TCR, and the seasonal variations in coincidence rates. Finally, Section 5 and Section 6 provide the discussion and conclusion, respectively.

2. STUDY AREA AND DATA

The study focuses on mainland India, which encompasses a wide range of climatic conditions, from the arid deserts of Rajasthan to the humid tropical regions of the Western Ghats, as well as distinct monsoon patterns that vary across regions (Figure 1). Previous studies have accounted for India's climatic heterogeneity using objective regionalization approaches (Guntu & Agarwal 2021; Rehana *et al.* 2024). However, analysis limited to predefined regions do not fully capture how temperature threshold exceedance and compound extremes vary continuously across regional boundaries. By analyzing mainland India as a connected spatial domain, this study identifies transition zones that extend beyond individual regions.

Precipitation in India typically begins with the pre-monsoon season, peaking during the Indian Summer Monsoon (ISM) from June to September. The pre-monsoon month of May contributes to about 6–14% of the total annual rainfall over the southern, northeastern, and eastern parts of India. In northeast India, many weather grid points exhibit a downward trend in rainfall, with the most pronounced reductions during the ISM and the least during the winter months. The decline in ISM rainfall ranges from 0.001 to 0.28 mm per decade, with the largest decrease recorded at grid points of Kailashahar over the period from 1901 to 2019 (Kuttippurath *et al.* 2021). Given the diverse climate and topography of the Indian subcontinent, generalizing or regionalizing studies across the country is a significant challenge. This complexity necessitates a comprehensive and nuanced approach when studying regional phenomena such as rainfall and heat waves. To effectively capture this climatic diversity within the gridded dataset, the study adopts ten homogeneous rainfall regions proposed by Guntu *et al.* (2020). These regions, delineated based on spatiotemporal rainfall variability, provide an appropriate framework for aggregating gridded data into climatically consistent zones. This regionalization helps reduce spatial heterogeneity and enables a more representative analysis of compounding heat waves and extreme precipitation across different parts of India.

The long-term gridded rainfall and maximum temperature records from 1951 to 2020 were provided by India Meteorological Department (IMD) at a 1° × 1° spatial resolution, covering the entire mainland India. The analysis spans two periods: a base period (1951–1980) and a recent period (1981–2020). Both the precipitation and the maximum temperature dataset are generated from a diverse network of 1803 and 395 gauging stations across India using an Inverse Distance Weighted (IDW) interpolation scheme. It has undergone extensive validation and inter-comparison with independent observations, as documented in previous studies (Pai *et al.* 2014) and further supported by Guntu & Agarwal (2021). These studies confirm that the IMD dataset robustly captures both spatial and temporal climate variability across India, including monsoon dynamics and diverse geographic settings. Comparative analyses with other gridded datasets have consistently demonstrated its reliability and highlighted its suitability as a reference dataset for hydroclimatic and climate extremes studies in India (Jena *et al.* 2020). All data pre-processing and analyses were performed using R (version 4.0.2), Python, and MATLAB, with Python coding executed via Google Collaboratory.

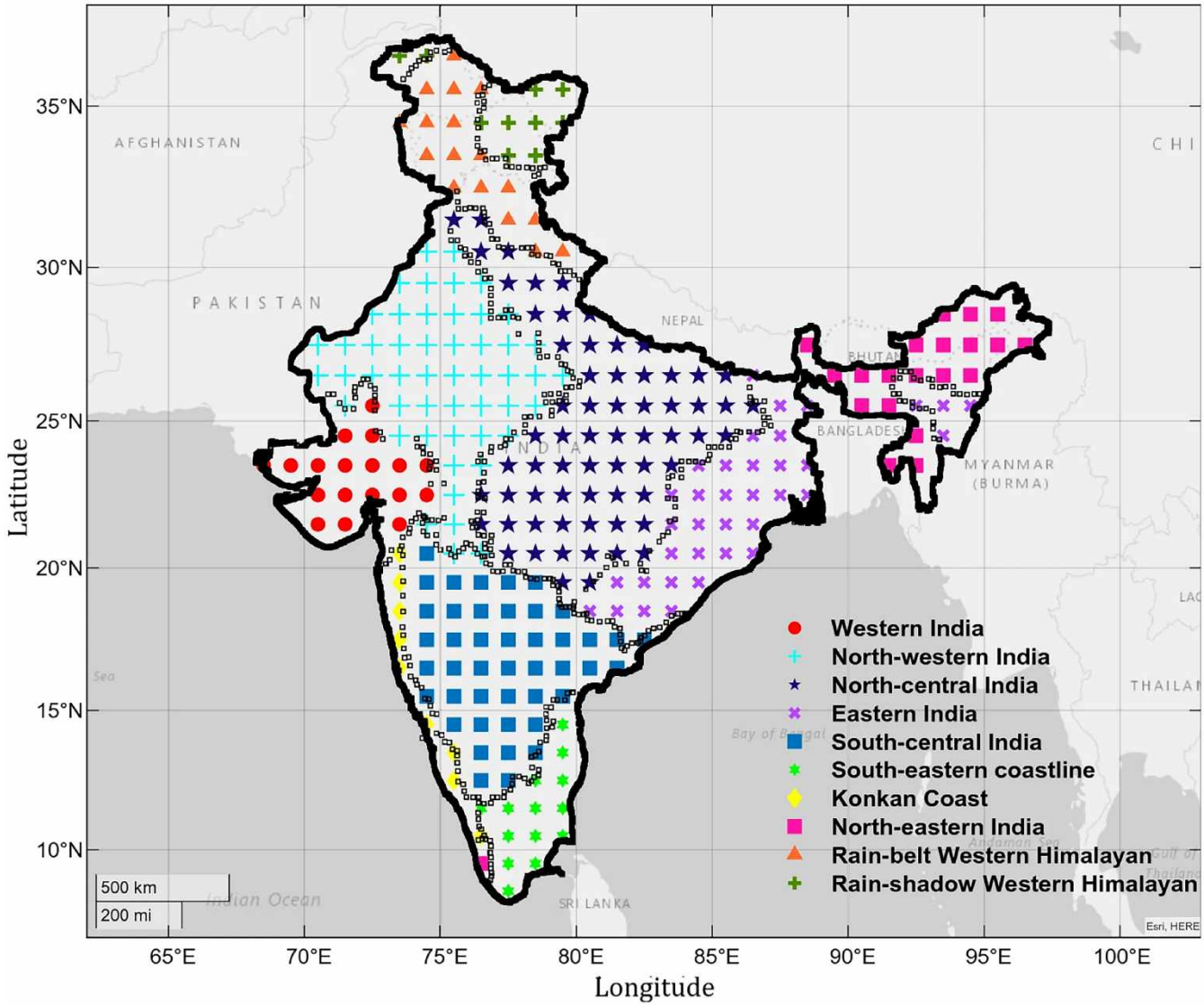

Figure 1 | Map illustrating 284 observation grid points across India, based on 1° × 1° resolution datasets from the India Meteorological Department. Climate classifications by Koppen depict semi-arid and desert zones in western and north-western India, humid subtropical regions in north-central and north-eastern India, tropical savannah in eastern India, semi-arid areas in south-central India, warm and humid subtropical climates in north-eastern India, tropical monsoon along the Konkan coast, and Alpine climates from the western Himalayas to the eastern Himalayas. Figure created using MATLAB's Mapping Toolbox and derived from Guntu & Agarwal (2021).

3. METHODS AND METHODOLOGY

3.1. Event coincidence analysis

ECA is a method used to identify simultaneous occurrences of events across two data series, referred to as coincidences. This simultaneity is defined by two key parameters: a user-defined time lag (τ) and a tolerance window (ΔT). The tolerance window (ΔT) accounts for these potential timing discrepancies by allowing a small range around the specified time, making ECA adaptable to real-world data with natural variability. In our study, we set the time lag (τ) to zero to observe cases where heavy rainfall follows immediately after a heat wave, allowing us to examine how quickly energy is exchanged between the atmosphere and hydrosphere in India (Siegmund *et al.* 2017). These parameters help ECA identify potentially significant statistical relationships and temporal coincidences between event time series, allowing for the detection of potential directional links or time-lagged precursors (Donges *et al.* 2016; Siegmund *et al.* 2017). In this analysis, one event series is

considered the respondent to the other. Here, we treat heat waves as the influencing event (type B) and analyze their potential impact on the timing of subsequent extreme heavy rainfall events (type A). Heat waves are identified as independent multi-day events (≥3 consecutive days above the 90th percentile) and treated as single Type B events with event timing assigned to the last day of each episode. This run-length event definition ensures that multi-day persistence is represented by a single event rather than by multiple correlated exceedances. For extreme precipitation (Type A events), consecutive exceedance days occurring within the tolerance window (ΔT) are collapsed into a single event, with the event time assigned to the first exceedance, thereby reducing short-term temporal autocorrelation.

ECA is then applied to these declustered event series, consistent with its event-based formulation (Odenweller & Donner 2020). By operating on independently defined extreme events, the ECA framework avoids artificial inflation of coincidence rates due to multi-day persistence, while preserving the physical duration of heatwave episodes. To quantify the interdependence between the two-event series, ECA utilizes two coincidence metrics: Precursor Coincidence Rate (PCR) and Trigger Coincidence Rate (TCR) (Donges *et al.* 2016).

3.1.1. Precursor coincidence rate

PCR represented by, $r_p(\Delta T,\ \tau)$, measures 'the fraction of A-type events that are preceded by at least one B-type event' (Siegmund *et al.* 2017), where precipitation is categorized as type-A events and heat waves are classified as type-B events. PCR is mathematically estimated as:

$$r_p(\Delta T,\ \tau) = \frac{1}{N_A}\sum_{i=1}^{N_A} H\left[\sum_{i=1}^{N_B} I_{[0,\ \Delta T]}((t_i^A - \tau) - t_j^B)\right] \tag{1}$$

Here, τ is the lag parameter between extreme precipitation and heat waves, N_A represents the number of A-type events, and ΔT denotes the temporal tolerance for preconditioning, typically set to two, five, or seven days. The Heaviside function H operates over the interval (0, ΔT), indicating how heat waves precondition extreme precipitation events. When $\Delta T = 0$, the inner sum simplifies to $\delta(t_i^A - \tau,\ t_j^B)$, where $\delta_{i,j}$ is the Kronecker delta, which equals 1 if both arguments are identical and 0 otherwise (Donges *et al.* 2016). The result of the inner sum indicates the coupling effect: a value of 0 suggests no coupling, while a value of 1 represents full (100%) coupling.

3.1.2. Trigger coincidence rate

TCR, represented as $r_t(\Delta T, \tau)$, quantifies 'the fraction of B-type events that are followed by at least one A-type event' (Donges *et al.* 2016; Siegmund *et al.* 2017). TCR can be mathematically derived as:

$$r_t(\Delta T,\ \tau) = \frac{1}{N_B}\sum_{i=1}^{N_B} H\left[\sum_{i=1}^{N_A} I_{[0,\ \Delta T]}((t_i^A - \tau) - t_j^B)\right] \tag{2}$$

where N_B is the number of events of B-type. The Heaviside function assesses whether the heat wave event being analyzed has a triggering effect after its conclusion, within the predefined specific temporal window.

This determines the proportion of heat wave events that act as a 'trigger' for the heavy precipitation event following the conclusion of the heat wave events, within the defined temporal window $\Delta T = 2$, 5 and 7 (immediate to moderate lags). This aspect of ECA calculation emphasizes the compound event scenario from the perspective of heat wave events. The analytical framework for computing the TCR and PCR is illustrated in Fig. S1, Fig. S2, and Figure 2.

While probabilistic and copula-based approaches quantify how the likelihood or intensity of one extreme changes conditional on another and estimate tail-dependence strength, they do not explicitly test whether one class of events systematically occurs before another in time. In contrast, PCR and TCR are event-based directionality metrics that directly quantify precursor–response relationships, allowing heatwaves to be identified as potential preconditioning drivers rather than merely statistically associated covariates. This distinction is particularly relevant for the Indian climate system, where land–atmosphere feedbacks, monsoon transitions, and synoptic persistence can generate short-lived but directional cascading hazards that are not explicitly resolved by dependence-based frameworks.

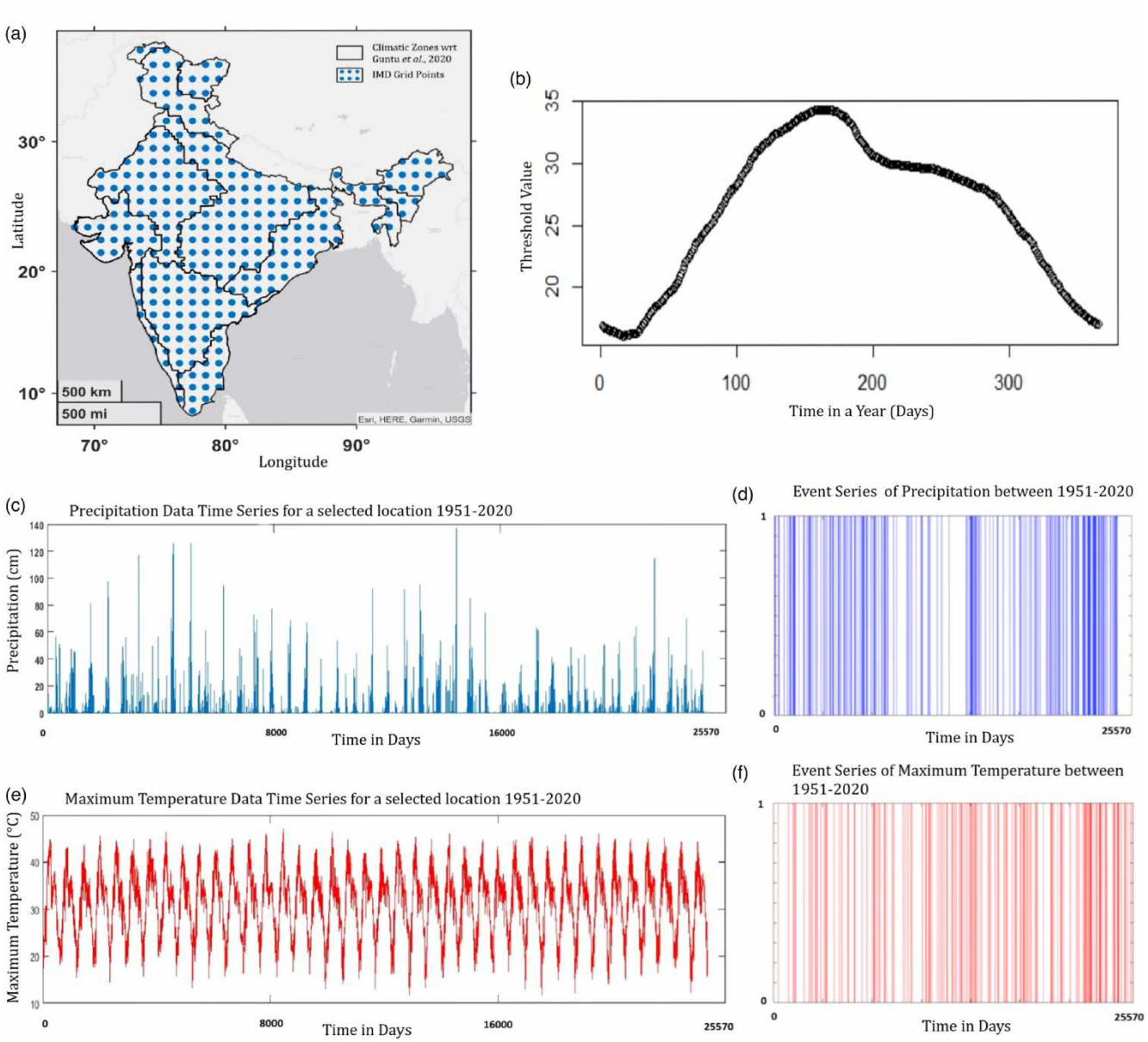

Figure 2 | Diagram illustrating the study methodology. Step 1: Selection of India's entire mainland as the study area. Step 2: Extraction of precipitation and maximum temperature time series from a representative grid point spanning India. Step 3: Identification of threshold records across 284 grid points. Step 4: Application of a 90th percentile cutoff and binarization of the data accordingly.

3.2. Significance test

Event series identification and coincidence counting were followed by a significance test using the ECA framework with a confidence level of 95% ($\alpha = 0.05$). This ensured that outcomes were not random. An essential criterion for applying the analytical significance test is that the product of the number of events and the tolerance window (ΔT) must be sufficiently small compared to the total period covered by the underlying observations, ensuring that the events being analyzed are rare.

The p-value from the analytical significance test provided by CoinCalc (Siegmund *et al.* 2016) indicates the likelihood that K_p or more coincidences are occurring by chance:

$$p(K_p) = \sum_{K'_p \geq K_p} P(K'_p) \tag{3}$$

Here, K_p represents the number of precursor coincidences obtained when event series A and B are compared. Similarly, the p-value for the corresponding significance test of the TCR, $r_t = K_t/N_B$ is obtained by interchanging N_A and N_B, and replacing K_p with K_t. In both instances, the null hypothesis states that the observed coincidences can be attributed to two independent series of randomly distributed events. If the calculated p-value is smaller than the predefined confidence level 'α', the null hypothesis is rejected. Only significant records meeting the criteria have been considered for results and analysis, while insignificant values (denoted as NA) have been excluded.

3.3. Methodology to identify compounding heat waves and heavy precipitation

We have 284 paired grid points of latitude and longitude to cover the entirety of India. For each grid point 'i', daily time series data for precipitation (P) and temperature (T) were converted into binary series (0 and 1). Here, 0 represents the absence of an event, and 1 signifies the occurrence of an event. These binary series were generated using the 90th percentile threshold for each grid point, applied to both precipitation and heat wave events. This threshold was calculated for each calendar day and location. This ensures that the methodology and the threshold calculation remain valid as they adapt to changes in both seasons and geographical locations. While this binary classification does not capture the relative intensity of extremes, it provides a consistent framework for analyzing the timing and co-occurrence of compound events. To ensure consistency, data for February 29th in leap years was excluded. A 31-day moving window was employed around the calendar days. This method was applied to both the base period (1951–1980) and the recent period (1981–2020). The daily time series for precipitation and temperature are denoted by $P_{90,\mathrm{i}}$ and $T_{90,\mathrm{i}}$, respectively, with observations for each $t = 1, 2, 3 \ldots T$, where T is the last time step of the observed record. The event time series $P_{90,\mathrm{i}}$ and $T_{90,\mathrm{i}}$ are defined as:

$$Y_i^P(t) = \begin{cases} 1, & \text{if } X^p > P_{90,\,i} \\ 0, & \text{otherwise} \end{cases} \tag{4}$$

$$Y_i^T(t) = \begin{cases} 1, & \text{if } X^T > T_{90,\,i} \\ 0, & \text{otherwise} \end{cases} \tag{5}$$

where $P_{90,\mathrm{i}}$ and $T_{90,\mathrm{i}}$ represent the site-specific percentile cutoffs for precipitation and temperature, respectively. This study uses the 90th percentile to retain the top 10% of daily values within the chosen timescale. Although, the 95th percentile is often used to define extreme precipitation events (Pendergrass 2018), and is widely employed in various studies to define extreme events (Leckebusch & Ulbrich 2004; Saidi *et al.* 2015; Sheridan & Lee 2018; Mondal *et al.* 2020). Yet, a recent study recommended using the 90th percentile limit for comparing numerical weather prediction precipitation extremes with the IMERG product at the daily scale (Da Silva *et al.* 2021). By focusing only on events of significant magnitude, the 10% criterion ensures an adequate number of events for describing coincidence rates. Percentile-based thresholds for identifying heat waves and intense rainfall periods have been shown to be reasonable and consistent with previous research (Zhai *et al.* 2005; Perkins & Alexander 2013; Casanueva *et al.* 2016; Sun *et al.* 2017; Perkins-Kirkpatrick & Lewis 2020). The detailed depiction of the overall methodology is given in Figure 2.

Building upon this threshold-based framework, extreme heat and precipitation events were characterized as follows. For each grid cell, a daily heat extreme was identified when the maximum temperature exceeded its 90th percentile threshold. To define a heat wave event, a minimum of three consecutive days of such exceedances was required at each grid point, consistent with the IMD definition adapted for gridded data. Similarly, extreme precipitation events were identified when daily rainfall exceeded the corresponding 90th percentile threshold for that grid and calendar day. Here, compound events are examined in the pre-conditioned sense, wherein antecedent heat wave conditions modify the background thermodynamic and land-atmosphere state under which extreme precipitation events occur. In the ECA, heat wave events (multi-day blocks) were paired with one-day extreme precipitation events occurring within the selected temporal tolerance window (ΔT) following the termination of heat wave episode.

3.4. Seasonal analysis of event coincidences

To assess the seasonal variability of compound heat wave–rainfall relationships, the ECA was performed separately for four climatological seasons of India: pre-monsoon (March–May; MAM), monsoon (June–September; JJAS), post-monsoon (October–November; ON), and winter (December–February; DJF). For each season, the PCR and TCR were computed using the

same temporal coincidence criteria and time lag ($\tau = 0$) described in Section 3.1. This approach allows us to identify how the statistical interrelationship between heat waves and heavy rainfall events varies seasonally across the study region.

This seasonal partitioning enables the identification of how the strength and direction of heat wave-rainfall associations vary under distinct large-scale circulation regimes. The different lengths of the seasonal time series (e.g. 2 months for ON vs. 4 months for JJAS) reflects the natural duration of the Indian climatological seasons as defined by the IMD. Similar approaches have been used in previous studies to examine the seasonal variability in temperature and rainfall extremes across India (Bhowmick *et al.* 2023; Salunke *et al.* 2023). These variations in seasonal length do not affect the statistical robustness of ECA since coincidence rates are normalized by the number of events per season rather than by the total time length.

4. RESULTS

This section illustrates the interdependence of heavy rainfall events and heat waves. For better understanding, we have categorized the results into different sections. Firstly, we delve into the spatiotemporal distribution of the PCR across India. Subsequently, we explore spatio-temporal relationship between heat waves and heavy rainfall events in India using TCR.

4.1. Spatiotemporal distribution of precursor coincidence rate

We computed the Precursor Coincidence Rate (PCR) between heat waves and heavy precipitation events in India during the recent study period (1981–2020) compared to the base period (1951–1980). We have selected 1980 to separate two time periods based on the studies on the climate shift around 1979–1980 and its implication on the ISM (Sabeerali *et al.* 2012; Sahana *et al.* 2015).

Figure 3(a) shows the PCR ($\boldsymbol{r_p}$; proportion of heat wave events that precede heavy rainfall events) calculated at 90% cut-off level (Section 3.3) providing insight into the reliability of the heat wave events as an indicator of the trigger event for heavy rainfall events. For instance, grid points with $\boldsymbol{r_p} > 0.30$ indicate that 30% of extreme precipitation events were preceded by heat wave events. These points are observed in the eastern borders of north-central India, around the northern borders of the Chota-Nagpur plateau region, northern banks of the Ganga basin in Bihar-Bengal border, towards the western borders of Rajmahal hills, and in the Katihar regions for $\Delta T = 2$ during the base period. Interestingly, as the temporal window increases from $\Delta T = 2$ to $\Delta T = 7$; we observe an increase in strong coupling at the south-central region, north-eastern India, rain-belt Himalayan region, eastern region, and the western tip of the western region, above the Bay of Kutch. The recent period also exhibits similar hotspot regions; however, these regions show a significant intensification in the strength of compound extremes' coupling, as indicated by an increased PCR. This suggests that the interactions between the climatic variables in these regions are amplifying, thereby highlighting heightened vulnerability to compound extreme events.

Additionally, results indicate a substantial increase in PCR from $\Delta T = 2$ to $\Delta T = 5$, followed by a less pronounced rise from $\Delta T = 5$ to $\Delta T = 7$ during both the base and recent periods. This suggests that the coupling strength of compound extremes intensifies significantly as the temporal window expands from $\Delta T = 2$ to $\Delta T = 5$. However, beyond $\Delta T = 5$, less pronounced intensification indicates the saturation effect in the coupling dynamics as the temporal window increases further.

Figure 3(b) presents boxplots showing that the median PCR has also enhanced in the recent time period compared to the base period, with increases also observed in the 25th and 75th percentiles, indicating spatial expansion of the PCR. Further, Figure 3(c) illustrates a rightward shift in the Cumulative Probability Distribution Curve in the recent period compared to the baseline period, reflecting strengthened coupling between heat waves and heavy precipitation with increasing temporal window. Quantitatively, for $\Delta T = 7$ days the fraction of grid points experiencing a heatwave within seven days prior to heavy rainfall nearly doubled from 13% during the base period (1951–1980) to 27% in the recent period (1981–2020). Consistently, the cumulative distribution for the recent period shows an increase in probability from ~8% for a 2-day temporal window to ~25% for a 7-day temporal window.

The observed increase in PCR across all temporal windows indicates a rising probability of precipitation events occurring shortly after heat waves, likely driven by enhanced atmospheric moisture and convective activity following intense heating. Heat waves elevate land surface temperatures, amplifying evaporation and increasing atmospheric moisture, which then creates favorable conditions for convective rainfall once temperatures cool or atmospheric dynamics shift. This pattern aligns with the Clausius–Clapeyron relationship, whereby warmer air can retain more moisture, setting up conditions conducive to rainfall (Trenberth *et al.* 2003). Similarly, Taylor *et al.* (2017) found that in sub-Saharan Africa, heat waves often lead to enhanced precipitation due to increased evaporation and moisture transport, resulting in rainfall shortly after the heat

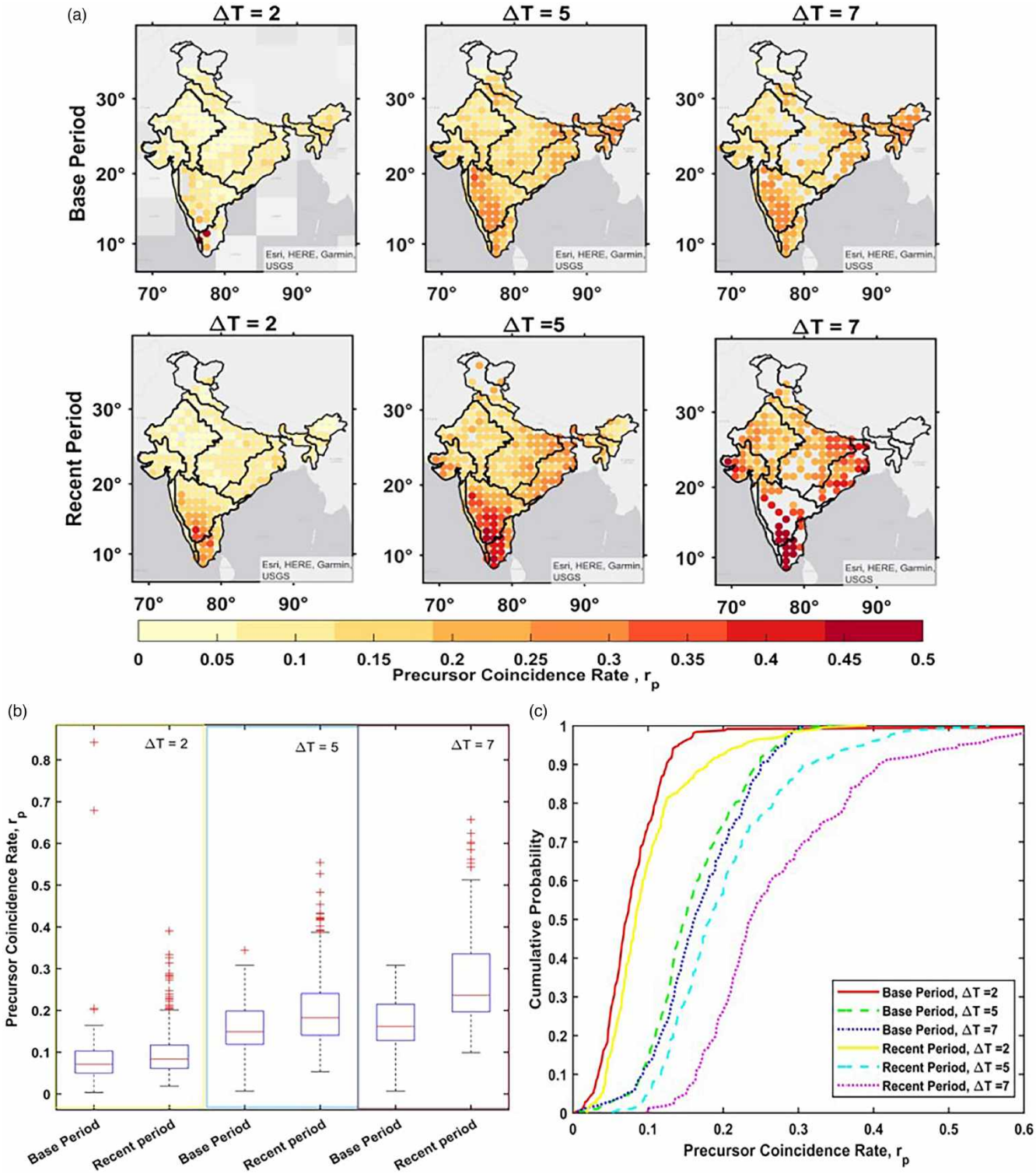

Figure 3 | (a) Spatiotemporal distribution of Precursor Coincidence Rate illustrating the coupling strength of heat waves and heavy precipitation events in India during the recent study period (1981–2020) compared to the base period (1951–1980). The analysis is conducted within predefined temporal windows of $\Delta T = 2$, 5, and 7 days, with statistically significant regions at the 0.05 level hatched on maps. (b) Box plots illustrating the comparison of Precursor Coincidence Rate for $\Delta T = 2$, 5, and 7 days between the base and recent periods. (c) Cumulative Probability Distributions for Precursor Coincidence Rate, comparing the recent study period (1981–2020) to the base period (1951–1980) across different temporal windows ($\Delta T = 2$, 5, and 7 days).

wave subsides. Li *et al.* (2025) documented a comparable sequence in East Asia, where high temperatures elevate atmospheric water vapor, producing significant precipitation events as atmospheric instability increases post-heat waves.

Further, to explicitly address the uncertainty arising from percentile-based event definitions and the choice of temporal tolerance window, PCR was recomputed using alternative thresholds of the 85th and 95th percentiles across temporal windows ranging from $\Delta T = 1$ to 10 days (Fig. S3–S6). At the stricter 95th percentile, PCR magnitudes are reduced across India relative to the 90th percentile due to the lower frequency of extreme events; however, the spatial patterns and temporal evolution remain consistent. In both the base and recent periods, PCR increases systematically with increasing ΔT, reaching a maximum around $\Delta T = 6$–7 days, after which the coupling strength weakens – more markedly in the recent period – indicating a reduced persistence of heatwave influence on subsequent rainfall beyond one week. A similar temporal evolution is observed at the 85th percentile threshold, where larger number of detected events leads to higher coupling magnitudes, yet the peak around a 7-day window and subsequent decline remain unchanged, confirming the robustness of the inferred heatwave–rainfall coupling to reasonable variations in threshold definition and timing.

4.2. Spatiotemporal distribution of trigger coincidence rate

Figure 4(a) (similar to Figure 3(a)) illustrates the Trigger Coincidence Rate (TCR; the proportion of heavy rainfall events following heat wave events) across different temporal intervals ($\Delta T = 2$, 5, 7 days) in India for the base period (1951–1980) and the recent study period (1981–2020). For $\Delta T = 2$, the pan-India scenario during the base period shows a TCR ranging from 0 to 0.02, with some coupling influences observed predominantly in the far northeast. TCR depicts increases over the eastern, far northeast, southern peninsular region, western Himalayan rain-belt of India for $\Delta T = 5$ during the base period, indicating a greater likelihood of heavy precipitation following heat waves in these areas. The high TCR in these regions is attributed to the regional variations in atmospheric moisture transport and topography that enhance convective activity following prolonged heat. Elevated moisture levels in these areas, coupled with complex orographic features in the Himalayas, create conditions conducive to rainfall events after a heat wave period. This effect is further intensified by the Clausius–Clapeyron relationship, which states that warmer air holds more moisture, setting the stage for heavy rainfall once atmospheric cooling or destabilization occurs (Trenberth *et al.* 2003). Further, minimal variations in the TCR intensity are observed as we move from $\Delta T = 5$ to $\Delta T = 7$.

In contrast, the recent period exhibits an intensified coupling phenomenon across the country, with an increasing temporal window. For $\Delta T = 5$, pronounced increase in TCR is evident towards the western part of India as compared to the base period. Over a 7-day period, the TCR for approximately 70% of grid points increased from 0.08 in the base period to 0.12 in the recent period. The observed increase in the TCR in India, particularly for longer temporal windows ($\Delta T = 7$ days), likely reflects the interplay between elevated land surface temperatures from heat waves and increased atmospheric moisture. During heat waves, the intense warming of the land surface enhances evaporation, boosting moisture in the lower atmosphere. Once conditions shift or temperatures decrease, this stored moisture can lead to convective rainfall, especially in regions where atmospheric instability and favorable synoptic conditions coincide with the end of the heat wave (Trenberth *et al.* 2003; Taylor *et al.* 2017; Dong *et al.* 2021).

Figure 4(b) presents a boxplot comparing TCR values for $\Delta T = 2$, 5, and 7 days between the base and recent periods. The median TCR value for $\Delta T = 2$ and 5 is slightly greater in base period compared to recent periods, reflecting the comparable intensity of TCR across both the time periods. However, spatial variability between the two periods for $\Delta T = 2$ and 5 leads to differences in the 25th and 75th percentile values for each period. Yet, for $\Delta T = 7$, median PCR has enhanced from base to recent period. This enhancement is attributed to a broader and more pronounced spatial distribution of TCR in the recent period, indicating a strengthening and expansion of regions experiencing compound climate extremes over longer temporal windows.

Figure 4(c) shows the Cumulative Probability Distributions, contrasting the recent study period (1981–2020) with the base period (1951–1980) across the temporal windows $\Delta T = 2$, 5, and 7 days. For $\Delta T = 2$, 5; the cumulative probabilities for the base and recent periods show less pronounced differences between the two periods. The most noticeable difference is observed for $\Delta T = 7$, with the recent period showing both higher TCR values and a broader distribution. These findings suggest that a rainfall event is more likely to develop and intensify over a 7-day period, followed by a heat wave, compared to shorter temporal windows of 2 or 5 days. This also indicates that shorter windows ($\Delta T = 2$, 5) capture the limited dynamics of the coupling during both periods.

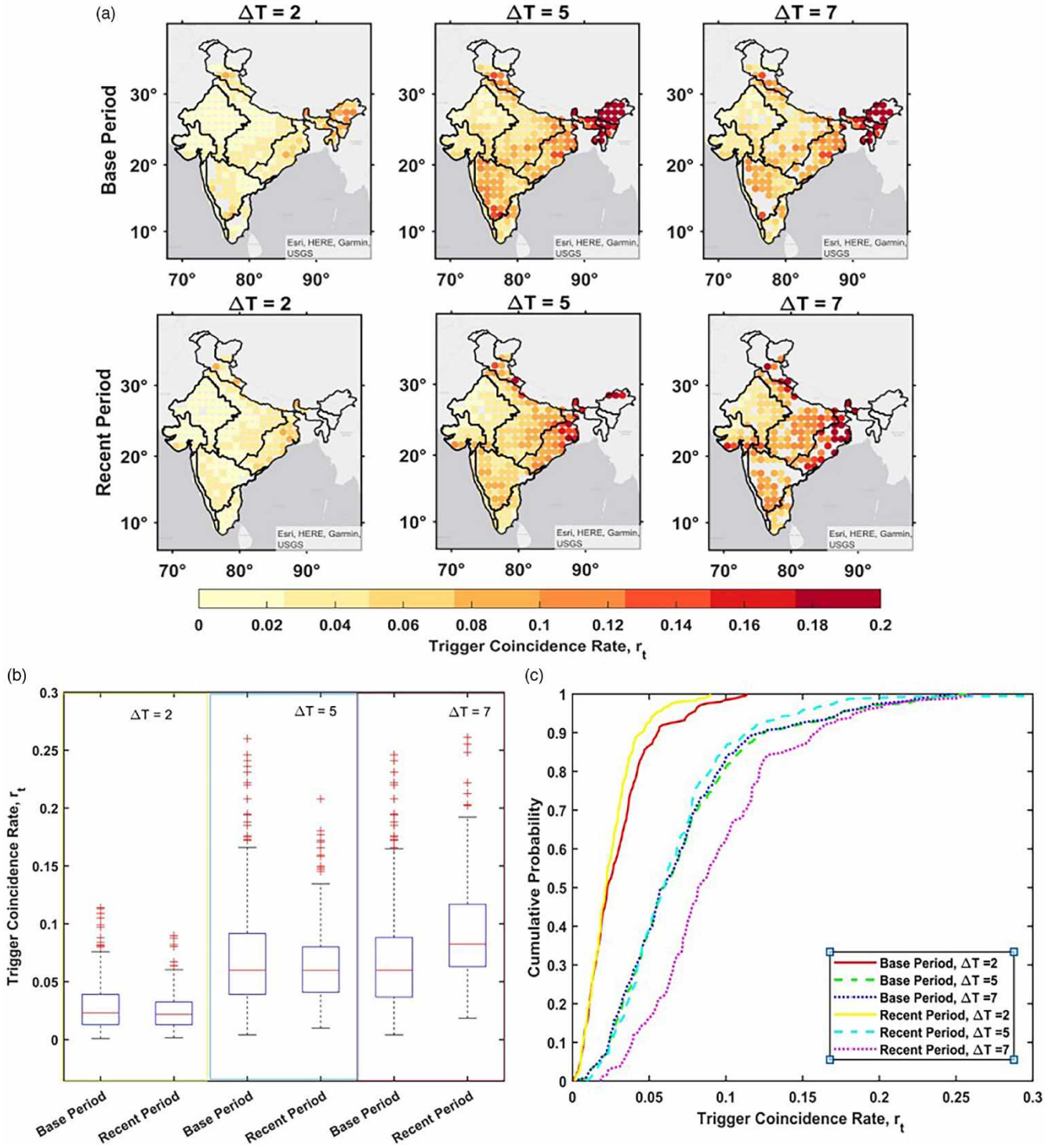

Figure 4 | (a) Spatiotemporal distribution of Trigger Coincidence Rate illustrating the coupling strength of heat waves and heavy precipitation events in India during the recent study period (1981–2020) compared to the base period (1951–1980). The analysis is conducted within predefined temporal windows of $\Delta T = 2$, 5, and 7 days, with statistically significant regions at the 0.05 level hatched on maps. (b) Box plots illustrating the comparison of Trigger Coincidence Rate for $\Delta T = 2$, 5, and 7 days between the base and recent periods. (c) Cumulative Probability Distributions for Trigger Coincidence Rate, comparing the recent study period (1981–2020) to the base period (1951–1980) across different temporal windows ($\Delta T = 2$, 5, and 7 days).

Further, a sensitivity analysis was performed for the TCR using alternative percentile thresholds (85th and 95th) and temporal windows ranging from $\Delta T = 1$ to 10 days (Fig. S7–S10). Consistent with PCR, TCR exhibits a systematic increase with increasing temporal window up to approximately 6–7 days, followed by a weakening at longer windows. While the absolute magnitude varies with threshold choice due to differences in event frequency, the temporal behaviour and spatial patterns remain robust.

4.3. Seasonal variations of precursor and trigger coupling of compound heat wave and heavy rainfall

The seasonal analysis of PCR and TCR offers intriguing insights into the changing dynamics of heat wave and heavy rainfall coupling across different periods in India. We have shown the results for both PCR and TCR across all four seasons i.e. winter (December-February; DJF), pre-monsoon (March-May; MAM), monsoon (June-September, JJAS) and post-monsoon (October-November; ON) using violin plots (Figures 5 and 6) across different time windows ($\Delta T = 2$, 5, and 7 days) and time periods (1950–1980 and 1981–2020).

4.3.1. Seasonal precursor coincidence analysis

For the winter season (DJF), the analysis shows that for a short temporal window ($\Delta T = 2$), the PCR in the base period ranges from 0 to 0.2, while the recent period extends this range up to 0.3 (Figure 5(a)). This increase suggests a stronger coupling between heat waves and subsequent rainfall in the recent period. The skewed distribution in recent years, with numerous outlier events, points to more extreme instances of this coupling, while the consistent median indicates a stable central tendency. The larger inter-quartile range (IQR) in the recent period for $\Delta T = 5$, 7 reflects greater variability, likely due to more frequent or intense shifts in atmospheric moisture availability following heat waves. Studies like Trenberth *et al.* (2003) confirm that rising temperatures enhance the atmosphere's moisture-holding capacity, which, under favorable conditions, can result in rainfall following heat extremes.

During the pre-monsoon season (MAM), similar trends to those observed in DJF emerge, indicating an intensified coupling between heat waves and rainfall events (Figure 5(c)). Notably, the recent period shows higher median PCR values, indicating a stronger likelihood of precipitation events shortly after heat waves (Figure 5(d)). The sharp rise in coupling strength from $\Delta T = 2$ to $\Delta T = 5$ suggests that pre-monsoon atmospheric dynamics, such as increasing humidity and convective potential, enhance the probability of rainfall in the days following a heat wave. This aligns with findings by Taylor *et al.* (2017), who observed that intense heat wave-induced evaporation increases atmospheric moisture, which, when coupled with convective conditions, can lead to rainfall events in subsequent days.

The monsoon season (JJAS) presents distinct characteristics compared to DJF and MAM. The recent period here shows a skewed distribution and wider IQR, indicating higher variability in heat wave-precipitation coupling (Figure 5(f)). However, unlike other seasons, the coupling strength is relatively weaker, likely because the atmosphere is already saturated with moisture during the monsoon, making additional moisture from heat waves less influential in triggering precipitation. Nevertheless, the presence of extreme cases in recent years suggests an increase in unusual heat wave-rainfall coupling events, possibly driven by monsoon variability and warming trends. Studies such as Dong *et al.* (2021) highlight that even during high-moisture seasons, intensified heat can occasionally lead to delayed convective processes, supporting our findings of heightened coupling in extreme cases.

In the post-monsoon season (ON), the analysis reveals consistent median PCR values for $\Delta T = 2$ and $\Delta T = 5$ between base and recent periods, indicating stability in short-term heat wave-precipitation coupling (Figure 5(h)). However, for $\Delta T = 7$, the recent period shows a dip in median PCR, along with significant skewness, suggesting a shift in coupling patterns over a longer time window. This skewed distribution implies that post-monsoon heat waves may have become less effective at preconditioning the atmosphere for delayed rainfall in recent years, likely due to seasonal shifts in atmospheric moisture transport as the monsoon retreats. This observation aligns with insights from Li *et al.* (2025), who found that post-monsoon climatic dynamics can alter the lagged effects of heat waves on precipitation due to changing large-scale circulation patterns.

4.3.2. Seasonal trigger coincidence analysis

During the winter season (DJF), the TCR median ranges between 0.02 and 0.04, with outliers extending up to 0.10–0.12 for $\Delta T = 2$ (Figure 6(a)). These outliers suggest sporadic but intense events where heavy rainfall closely follows heat waves. This seasonal variability may arise from relatively stable atmospheric conditions of winter, which occasionally destabilize due to intense heating, promoting convective rainfall. Interestingly, the highest density of TCR values appears around 0.02, differing from the median, indicating a frequent but low intensity coupling pattern. The consistency in the lower IQR range implies a

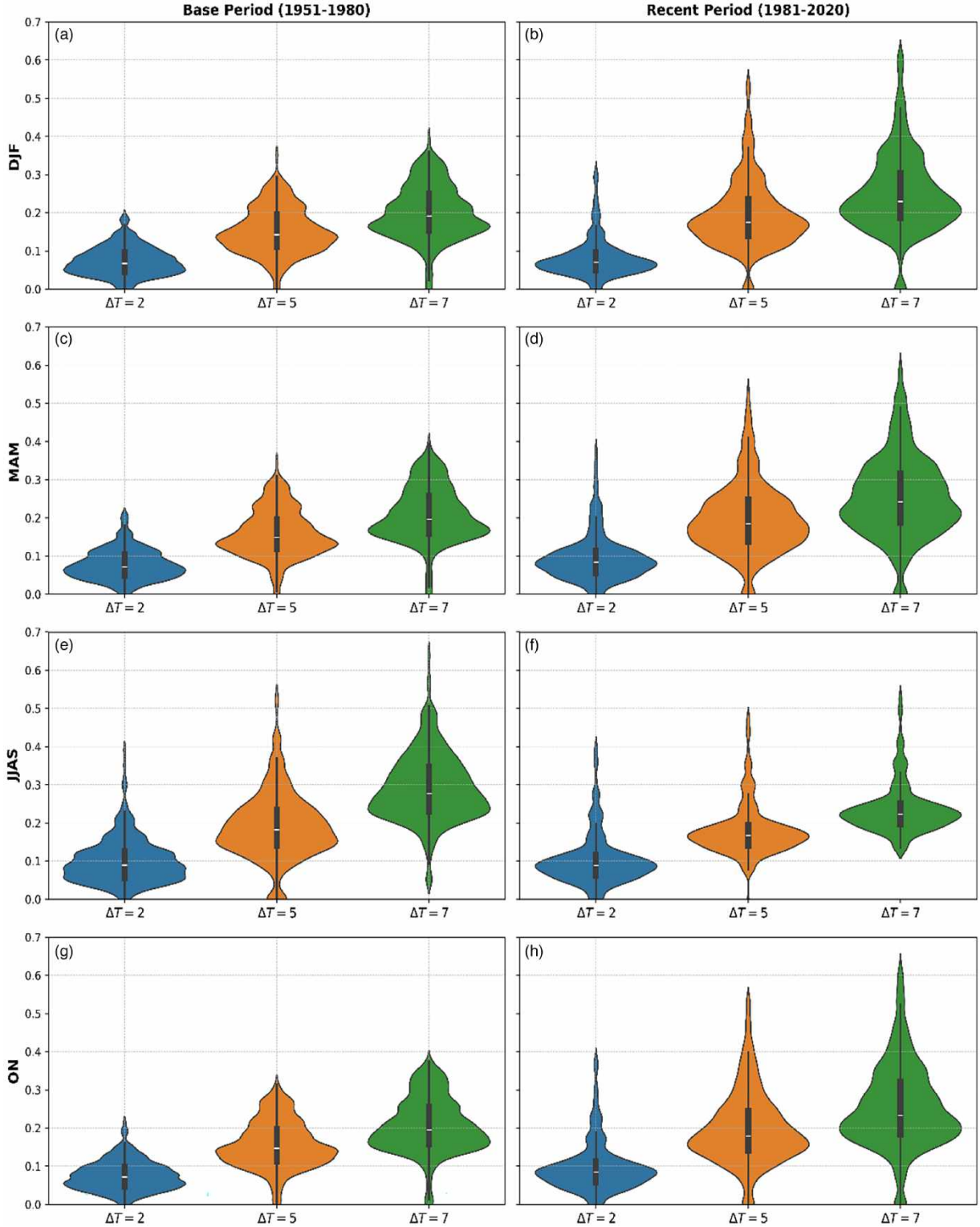

Figure 5 | Violin plots showing the Precursor Coincidence Rate coupling comparison for different time windows ($\Delta T = 2$, 5, and 7) for winter (DJF); pre-monsoon (MAM); monsoon (JJAS) and post-monsoon (ON) for both base period (1950–1980) and recent period (1981–2020).

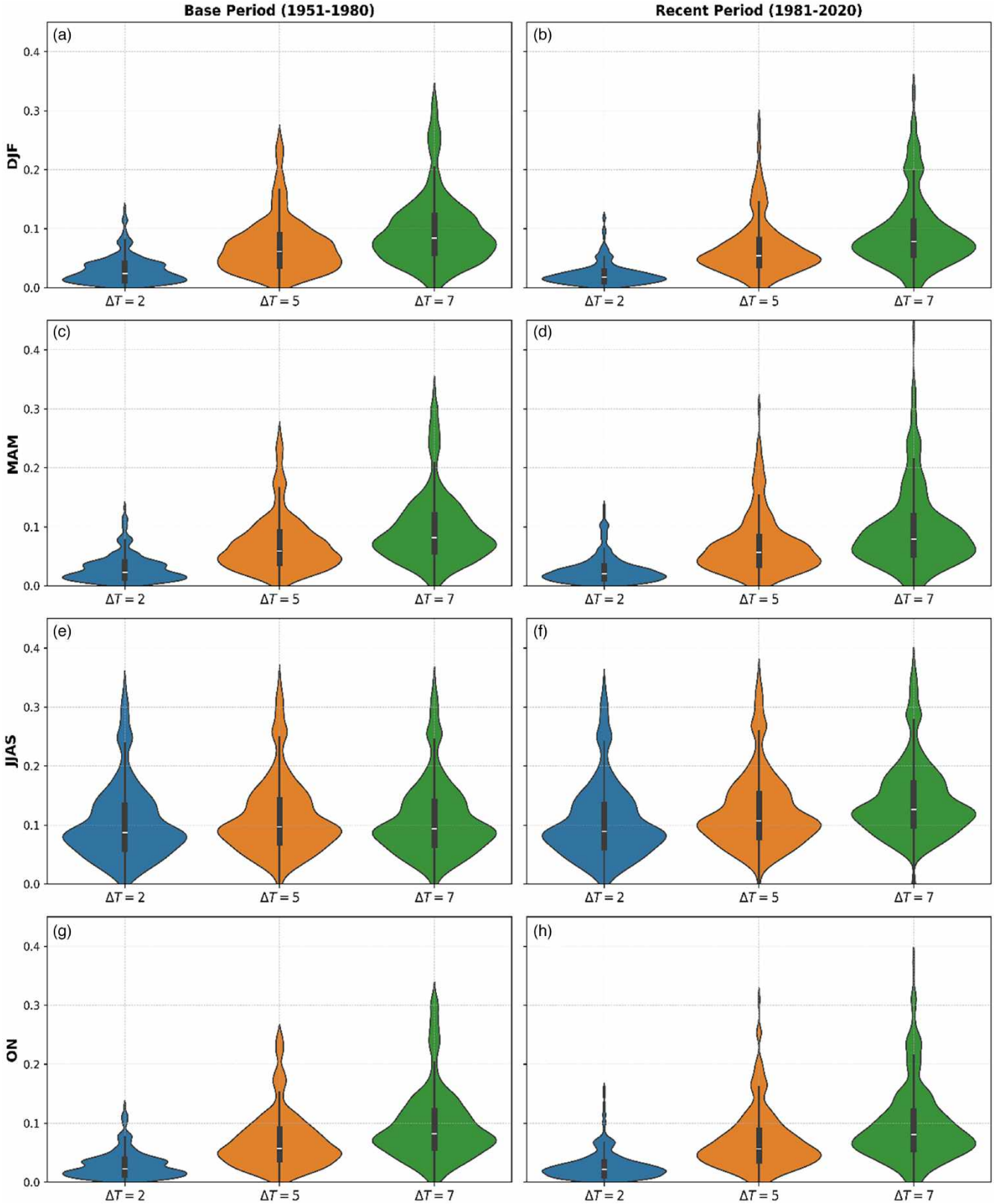

Figure 6 | Violin plots showing the Trigger Coincidence Rate for different time windows ($\Delta T = 2$, 5, and 7) for Winter (DJF); Pre-monsoon (MAM); Monsoon (JJAS) and Post Monsoon (ON) for both base period (1950–1980) and recent period (1981–2020).

relatively stable TCR coupling in winter, suggesting that heat wave-induced rainfall events are less variable but more isolated during this season. Similar observations have been noted by Trenberth *et al.* (2003), who found that atmospheric moisture-holding capacity during cooler months can lead to rainfall when intense warming disrupts stability.

The pre-monsoon season (MAM) exhibits an increase in TCR density from $\Delta T = 2$ to $\Delta T = 5$, particularly during the base period, suggesting a heightened frequency of coupling between heat waves and subsequent rainfall events (Figure 6(c)). This transitional climate of MAM, characterized by rising temperatures and increased atmospheric moisture, likely enhances the probability of rainfall following heat waves. Notably, the TCR median is higher in the recent period, pointing to an intensified likelihood of rainfall after heat waves. The expanded IQR in recent years implies increased variability in heat wave-induced rainfall events, likely driven by regional climate shifts. This finding aligns with Taylor *et al.* (2017), who observed that in transitional seasons, heat waves heighten evaporation and atmospheric moisture, setting favorable conditions for precipitation.

During the monsoon season (JJAS), the TCR values display remarkable uniformity, with the median and maximum density aligning, suggesting stable coupling between heat waves and rainfall events (Figure 6(e)). This uniformity likely results from the already high atmospheric moisture levels during the monsoon, where additional moisture from heat waves may only marginally impact rainfall likelihood. However, outliers in the range of 0.25–0.35 highlight instances of extreme rainfall following heat waves, pointing to occasional anomalies potentially driven by localized convective storms. This pattern of stable coupling with sporadic extremes may reflect the strong but variable nature of monsoon in India. Dong *et al.* (2021) documented similar patterns, noting that monsoonal moisture saturation dampens coupling strength but allows extreme cases during peak convective activity.

The post-monsoon season (ON) exhibits distinct differences between the base and recent periods, with the recent period showing an abrupt transition from $\Delta T = 2$ to $\Delta T = 5$, unlike the gradual shift observed in the base period (Figure 6(g) and 6(h)). This abrupt change could reflect altered atmospheric dynamics in recent years, where post-monsoon heat waves contribute to short-term atmospheric moisture but are less effective in sustaining prolonged coupling. A notable increase in the TCR median during the recent period suggests a shift toward more intense coupling dynamics, possibly due to lingering monsoonal moisture that can be triggered by post-monsoon heat waves. This seasonal shift aligns with observations by Li *et al.* (2025), who found that post-monsoon heat wave and rainfall dynamics are increasingly influenced by seasonal transition processes, which modify atmospheric conditions.

5. DISCUSSION

This study employs ECA to quantify the relationship between heat waves and heavy rainfall events across India from 1951 to 2020, leveraging key metrics – Precursor Coincidence Rate (PCR) and Trigger Coincidence Rate (TCR)—to understand the complex interactions between these extremes. Indeed, a multitude of research attributes these rises in compound climate extremes to shifts in land-ocean-atmosphere processes driven by changing temperatures over both land and sea surfaces.

Our investigation using the PCR reveals key insights into the preconditioning role of heat waves in inducing heavy rainfall across different regions in India. Notably, hotspot regions, such as south-central India, north-eastern India, the Himalayan rain belt, and eastern India, show strong coupling between these extremes, particularly as the temporal window extends from $\Delta T = 2$ to $\Delta T = 7$. These areas show that approximately 30% of extreme precipitation events were preceded by heat waves, underscoring the importance of understanding spatiotemporal dynamics in these coupled events. In south-central India, strong pre-monsoon heating and proximity to the Bay of Bengal and Arabian Sea promote intense convection when moist air masses intrude inland. While northeastern India, characterized by complex topography and persistent moisture influx from the Bay of Bengal, experiences frequent transitions from dry heat to convective downpours as the monsoon advances. Along the Himalayan foothills, orographic lifting and synoptic-scale moisture convergence amplify these interactions, often resulting in flash floods and landslides.

The increase in median PCR and widening of the inter-quartile range (25th to 75th percentiles) in recent years indicate that these coupled extremes have intensified and expanded spatially. This pattern aligns with findings by Fischer & Knutti (2015), who reported that rising temperatures increase atmospheric water-holding capacity, thereby enhancing the potential for extreme rainfall following heatwaves. This is further corroborated by recent assessments, such as Rehana *et al.* (2024), who identified a significant rise in warm/wet compound extremes across India (0.3% per decade) using monthly standardized indices. While those monthly assessments identify broad seasonal risks, our grid-point ECA reveals

event-scale dyanamics – specifically showing that the inter-quartile range of PCR is widening, indicating that these couplings are becoming more erratic and spatially extensive than previously recognized. Further, the heightened TCR at longer temporal windows ($\Delta T = 7$) further suggests that prolonged heat episodes can facilitate gradual atmospheric moistening, setting the stage for delayed but intense precipitation events.

Multiple feedback mechanisms can explain these statistical couplings. Prolonged surface heating depletes soil moisture and weakens evaporative cooling, producing positive land-atmosphere feedback that intensifies subsequent convection once moisture becomes available. Elevated surface temperatures enhance evapotranspiration and boundary-layer moisture, increasing convective available potential energy (CAPE) and promoting instability (Trenberth *et al.* 2014). This aligns with Falga & Wang (2022), who identified convective instability as a primary driver for the frequency of precipitation extremes in several Indian regions. Such preconditioning likely destabilizes the atmosphere, explaining why short, intense heatwaves are often followed by torrential rainfall. While Rehana *et al.* (2024) utilized the 12-month SPEI to link thermal anomalies with moisture deficits or surpluses, our use of daily precipitation extremes captures the immediate convective response. Similar mechanisms have been observed during notable Indian flood events, where antecedent heat stress was followed by intense rainfall sequences – called 'hot–wet' extremes – exacerbating crop and infrastructure losses. The spatial overlap between strong heat–rainfall coupling and historically flood-prone regions such as the Indo-Gangetic Plain and the northeastern hill states underscores the real-world implications of our findings.

Seasonal TCR analysis highlights how coupling dynamics between heat waves and rainfall vary across different seasons. In winter (DJF), the base period shows a slightly denser TCR distribution at $\Delta T = 5$, with a median around 0.10, while the recent period displays pronounced skewness and more outliers, indicating more frequent extreme events. During pre-monsoon (MAM), the coupling strength increases, with higher median values in recent years, suggesting intensified coupling. In monsoon (JJAS), TCR values are more uniform, reflecting consistent moisture interactions, though sporadic extreme events are evident. The post-monsoon season (ON) reveals distinct patterns, with recent years showing an abrupt change in coupling from $\Delta T = 2$ to $\Delta T = 5$, which may reflect shifts in atmospheric moisture dynamics due to lingering monsoonal moisture (Li *et al.* 2025).

Our study highlights the increasing likelihood of heavy rainfall following shorter, more intense heat waves, driven by elevated atmospheric water vapor and convective potential. This supports climate scientists' assertions that as temperatures rise, extreme precipitation events become more frequent and intense due to the increased water-holding capacity of warmer air, with each 1 °C increase allowing the atmosphere to hold approximately 7% more water (IPCC 2021). This research underscores the growing need for climate adaptation and mitigation strategies focused on managing compound extremes, particularly in regions with high exposure to both heat waves and heavy rainfall.

These compound events pose serious risks to agriculture, water management, and urban infrastructure. In the Indo-Gangetic Plain and peninsular India, heat stress during crop growth stages is frequently followed by inundation during harvest, undermining food security. Major metropolitan areas such as Delhi, Mumbai, and Chennai face cascading impacts – rising energy demand during heatwaves and severe stormwater flooding afterward. These findings reinforce the need for integrated adaptation frameworks that jointly assess heat and rainfall risks rather than treating them as isolated hazards.

From an operational perspective, PCR and TCR provide event-based indicators that can support impact-based forecasting and multi-hazard early warning systems. TCR allows heatwave forecasts to be used as early lead-time signals for flood preparedness and adaptive reservoir management. Also, there is risk to transport infrastructure, as prolonged heat weakens asphalt and railway tracks, increasing susceptibility to washouts during subsequent heavy rainfall – a combined 'thermal–hydro' stress identified as a key adaptation challenge for Asian transport systems (Regmi & Hanaoka 2011).

PCR is equally relevant for public health and long-term planning, as transitions from extreme heat to wet conditions create favorable breeding windows for disease vectors, with temperature–humidity lags linked to malaria and dengue transmission in Indian hotspots such as West Bengal, Odisha, and Assam (Bhattacharya *et al.* 2006; Dhiman *et al.* 2010; Lambiase & Rizzo 2016). In urban and basin-scale contexts, rising PCR values imply enhanced runoff due to heat-induced soil drying and hydrophobicity, necessitating climate-adaptive drainage design and flood control infrastructure. Integrating PCR for infrastructure planning and TCR for real-time alerts into Multi-Hazard Early Warning Systems (Krishnan *et al.* 2025) would enable a shift from single-hazard forecasting towards compound-risk–informed preparedness across water, health, and infrastructure sectors. Early warning systems, resilient crop planning, and improved drainage infrastructure could substantially reduce vulnerability to these escalating compound events.

While this study provides valuable insights, several limitations should be noted. First, our analysis highlights regions with strong heat wave-rainfall coupling, it does not account for external factors such as land use changes, urbanization, or socio-economic variables that could influence observed patterns. Second, the ECA configuration adopted here uses a fixed $\tau = 0$, which captures near-synchronous co-occurrence of extremes but does not explicitly resolve lagged or sequential dependence between heat waves and precipitation events. A systematic exploration of τ sensitivity represents an important avenue for future research. Third, the temporal resolution of our investigation is limited by the availability of daily data, potentially missing short-lived interactions. The spatial resolution may also not fully capture localized topographical effects and microclimate variations. Finally, this research primarily examines statistical relationships, suggesting the need for further studies to investigate underlying physical mechanisms and causal pathways. Addressing these limitations would enhance the understanding and management of compound climate extremes.

6. CONCLUSION

The compounding of heat waves and extreme precipitation events poses a growing hydro-climatic risk across India. This study reveals that while TCR decreased in recent period for shorter temporal windows ($\Delta T = 2$ and $\Delta T = 5$), it increased significantly – by 50% across 70% of grid points – for a longer temporal window ($\Delta T = 7$). The widespread increase in PCR further indicates that heatwaves are increasingly acting as precursors to rainfall extremes across large parts of south-central India, northeastern India, and the Himalayan foothills. In these regions, heat-induced soil drying and surface hardening can enhance runoff efficiency when intense rainfall follows, increasing the risk of flash floods and landslides, as observed during recent pre-monsoon and monsoon transition events in northeast India and the Himalayan rain-belt (Dilip *et al.* 2025). By explicitly resolving precursor and triggering relationships between heatwaves and extreme rainfall, this study provides the process-level understanding required to interpret emerging impact-based evidence. Recent assessments indicate that rainfall events following humid heatwaves result in several-fold increases in inundation extent and population exposure in Chennai (Ganguli *et al.* 2025), underscoring that the compound-event sequencing identified here has hazardous societal consequences.

Further, seasonal TCR analysis illustrates the complex and variable nature of heat wave-precipitation coupling across different times of the year. During the pre-monsoon season (MAM), coupling strength intensifies, while winter (DJF) and post-monsoon (ON) show more skewed distributions and increased extreme events in the recent period. The monsoon season (JJAS) exhibits weaker coupling, likely due to high ambient moisture, yet sporadic extreme events persist. The intensified heat wave-precipitation events exacerbate risks of flash floods, soil erosion, and reduced crop yields, especially during critical agricultural periods, posing substantial challenges for stakeholders.

These findings underscore the importance of compound extremes as a critical factor in linking heat waves to subsequent precipitation, highlighting their severe impacts on India's water and climate systems. The intensified hot–wet interactions can disrupt hydrological balance, strain water resources, and exacerbate flood and drought risks in quick succession – posing significant challenges for agriculture, urban water supply, and ecosystem stability. Therefore, integrating insights from compound event analysis into water management, climate adaptation, and early warning frameworks is vital. Developing targeted adaptation strategies – specifically utilizing PCR to predict vector-borne disease transmission windows (Bhattacharya *et al.* 2006) and TCR to inform climate-resilient infrastructure design (Regmi & Hanaoka 2011) will enhance national resilience. In addition, promoting efficient irrigation practices could help mitigate the feedback loops driving moist heat stress (Ambika & Mishra 2022), thereby reducing the severity of these compound extremes across the Indian mainland.

ACKNOWLEDGEMENTS

The authors acknowledge the funding from the Anusandhan National Research Foundation (CRG/2023/003449) at the Indian Institute of Technology, Roorkee. The authors express appreciation and gratitude to all members of the HydroClimX Lab at the Department of Hydrology, Indian Institute of Technology, Roorkee for their fruitful discussions and valuable contributions to this work. Additionally, the authors acknowledge the assistance provided by Mr Debjit Paul, Centre for Atmospheric Sciences, Indian Institute of Technology, Delhi for his support with computational aspects of the project.

CREDIT AUTHORSHIP CONTRIBUTION STATEMENT

Swarnendu Saha: Conceptualization, Data curation, Formal analysis, Investigation, Methodology, Resources, Software, Writing – original draft.

Divya Sardana: Investigation, Resources, Software, Supervision, Writing – review & editing.
Ashish Manoj J: Investigation, Methodology, Resources, Software, Supervision, Writing – review & editing.
Ankit Agarwal: Conceptualization, Project administration, Funding acquisition, Supervision, Writing – review & editing

DATA AVAILABILITY STATEMENT

All relevant data are included in the paper or its Supplementary Information.

CONFLICT OF INTEREST

The authors declare there is no conflict.

REFERENCES

Agha Kouchak, A., Chiang, F., Huning, L. S., Love, C. A., Mallakpour, I., Mazdiyasni, O., Moftakhari, H., Papalexiou, S. M., Ragno, E. & Sadegh, M. (2020) Climate extremes and compound hazards in a warming world, *Annual Review of Earth and Planetary Sciences*, **48**, 519–548. doi:10.1146/annurev-earth-071719-055228.

Ambika, A. K. & Mishra, V. (2022) Improved water savings and reduction in moist heat stress caused by efficient irrigation, *Earth's Future*, **10**, e2021EF002642. https://doi.org/10.1029/2021EF002642.

Bansal, A., Cherbuin, N., Davis, D. L., Peek, M. J., Wingett, A., Christensen, B. K., Carlisle, H., Broom, M., Schoenaker, D. A. J. M., Dahlstrom, J. E., Phillips, C. B., Vardoulakis, S., Nanan, R. & Nolan, C. J. (2023) Heatwaves and wildfires suffocate our healthy start to life: time to assess impact and take action, *The Lancet Planetary Health*, **7** (8), e718–e725. https://doi.org/10.1016/s2542-5196(23)00134-1.

Barriopedro, D., García-Herrera, R., Ordóñez, C., Miralles, D. G. & Salcedo-Sanz, S. (2023) Heat waves: physical understanding and scientific challenges, *Reviews of Geophysics*, **61**, e2022RG000780. 10.1029/2022RG000780.

Bhattacharya, S., Sharma, C., Dhiman, R. C. & Mitra, A. P. (2006) Climate change and malaria in India, *Current Science*, **90** (3), 369–375.

Bhowmick, M., Sahany, S. & Das, A. K. (2023) Recent changes in the climatological characteristics of daily contiguous rain areas over India, *npj Climate and Atmospheric Science*, **6**, 178. https://doi.org/10.1038/s41612-023-00464-6.

Casanueva, A., Kotlarski, S., Herrera, S., Fernández, J., Gutiérrez, J. M., Boberg, F., Colette, A., Christensen, O. B., Goergen, K., Jacob, D., Keuler, K., Nikulin, G., Teichmann, C. & Vautard, R. (2016) Daily precipitation statistics in a EURO-CORDEX RCM ensemble: added value of raw and bias-corrected high-resolution simulations, *Climate Dynamics*, **47** (3), 719–737. doi:10.1007/s00382-015-2865-x.

Centre for Research on the Epidemiology of Disasters (CRED) (2020) *Natural Disasters 2019*. Brussels: CRED.

Da Silva, N. A., Webber, B. G. M., Matthews, A. J., Feist, M. M., Stein, T. H. M., Holloway, C. E. & Abdullah, M. F. A. B. (2021) Validation of GPMIMERG extreme precipitation in theMaritime continent by station and radar data, *Earth and Space Science*, **8**, e2021EA001738. https://doi.org/10.1029/2021EA001738.

Dhiman, R. C., Pahwa, S. & Dash, A. P. (2010) Climate change and malaria in India: interplay between temperature and mosquitoes, *Regional Health Forum*, **12** (1).

Dilip, K. N., Vegad, U. & Mishra, V. (2025) Drivers of flash floods in the Indian sub-continental river basins, *npj Natural Hazards*, **2**, 62. https://doi.org/10.1038/s44304-025-00121-3.

Donat, M. G., Lowry, A. L., Alexander, L. V., O'Gorman, P. A. & Maher, N. (2016) More extreme precipitation in the world's dry and wet regions, *Nature Climate Change*, **6** (5), 508–513. doi:10.1038/nclimate2941.

Dong, N., Wang, X., Li, Y., Gao, L. & Zhang, J. (2021) Compound extremes of heat waves and heavy precipitation in China: observed linkage and associated large-scale circulations, *Science of the Total Environment*, **750**, 141681. doi:10.1016/j.scitotenv.2020.141681.

Donges, J. F., Schleussner, C. F., Siegmund, J. F. & Donner, R. V. (2016) Event coincidence analysis for quantifying statistical relationships between event time series, *The European Physical Journal Special Topics*, **225**, 471–487. doi:10.1140/epjst/e2015-50233-y.https://doi.org/10.48550/arXiv.1508.03534.

Falga, R. & Wang, C. (2022) The rise of Indian summer monsoon precipitation extremes and its correlation with long-term changes of climate and anthropogenic factors, *Scientific Reports*, **12**, 11985. https://doi.org/10.1038/s41598-022-16240-0.

Fischer, E. M. & Knutti, R. (2015) Anthropogenic contribution to global occurrence of heavy-precipitation and high-temperature extremes, *Nature Climate Change*, **5** (6), 560–564. doi:10.1038/nclimate2617.

Ganguli, P. & Merz, B. (2024) Observational evidence reveals compound humid heat stress-extreme rainfall hotspots in India, *Earth's Future*, **12** (2), e2023EF004074. doi:10.1029/2023EF004074.

Ganguli, P., Nithila Devi, N., Apel, H., Vorogushyn, S., Jena, P. P., Chatterjee, C. & Merz, B. (2025) Growing pluvial flood hazard and exposure from heatwave-preconditioned rainfall extremes in Chennai Metropolitan Area, India, *Geophysical Research Letters*, **52** (17), e2025GL115795. doi:10.1029/2025GL115795.

Guntu, R. K. & Agarwal, A. (2021) Disentangling increasing compound extremes at regional scale during Indian summer monsoon, *Scientific Reports*, **11**, 16447. doi:10.1038/s41598-021-95775-0.

Guntu, R. K. & Agarwal, A. (2024) Compound dry and hot extremes: A review and future research pathways for India, *Journal of Hydrology*, **635**, 131199. https://doi.org/10.1016/j.jhydrol.2024.131199.

Guntu, R. K., Maheswaran, R., Agarwal, A. & Singh, V. P. (2020) Accounting for temporal variability for improved precipitation regionalization based on self-organising maps coupled with information theory, *Journal of Hydrology*, **590**, 125236. https://doi.org/10.1016/j.jhydrol.2020.125236.

Hao, Z., Singh, V. & Hao, F. (2018) Compound extremes in hydroclimatology: a review, *Water*, **10**, 718. doi:10.3390/w10060718.

IPCC (2021) *Climate Change 2021: the Physical Science Basis. Contribution of Working Group I to the Sixth Assessment Report of the Intergovernmental Panel on Climate Change*. Cambridge, UK: Cambridge University Press.

Jena, P., Garg, S. & Azad, S. (2020) Leckebuschperformance analysis of IMD high-resolution gridded rainfall (0.25° × 0.25°) and satellite estimates for detecting cloudburst events over Northwest Himalaya, *Journal of Hydrometeorology*, **21**, 1549–1569. https://doi.org/10.1175/JHM-D-19-0287.1.

Kotz, M., Levermann, A. & Wenz, L. (2022) The effect of rainfall changes on economic production, *Nature*, **601** (7892), 223–227. https://doi.org/10.1038/s41586-021-04283-8.

Krishnan, R., Dhara, C., Horinouchi, T., Gotangco Gonzales, C. K., Dimri, A. P., Shrestha, M. S., Swapna, P., Roxy, M. K., Son, S.-W., Ayantika, D. C., Cruz, F. A. T. & Qiao, F. (2025) Compound weather and climate extremes in the Asian region: science-informed recommendations for policy, *Frontiers in Climate*, **6**, 1504475. https://doi.org/10.3389/fclim.2024.1504475.

Kuttippurath, J., Murasingh, S., Stott, P. A., Sarojini, B. B., Jha, M. K., Kumar, P., Nair, P. J., Varikoden, H., Raj, S., Francis, P. A. & Pandey, P. C. (2021) Observed rainfall changes in the past century (1901–2019) over the wettest place on Earth, *Environmental Research Letters*, **16** (2), 024018. doi:10.1088/1748-9326/abcf78.

Lambiase, L. & Rizzo, E. (2016) Health impact of climate change in India: a review of the literature, *Annali dell'Istituto Superiore di Sanità*, **52** (3), 423–429.

Leckebusch, G. C. & Ulbrich, U. (2004) On the relationship between cyclones and extreme windstorm events over Europe under climate change, *Global and Planetary Change*, **44** (1–4), 181–193. https://doi.org/10.1016/j.gloplacha.2004.06.011.

Li, D., Yuan, J. & Kopp, R. E. (2020) Escalating global exposure to compound heat-humidity extremes with warming, *Environmental Research Letters*, **15**, 064003. doi:10.1088/1748-9326/ab7d04.

Li, J., Wang, S., Zhu, J., Wang, D. & Zhao, T. (2025) Accelerated shifts from heatwaves to heavy rainfall in a changing climate, *npj Climate and Atmospheric Science*, **8**, 214. https://doi.org/10.1038/s41612-025-01113-w.

Luo, M. & Lau, N.-C. (2021) Increasing human-Perceived heat stress risks exacerbated by urbanization in China: a comparative study based on multiple metrics, *Earth's Future*, **9**, e2020EF001848. doi:10.1029/2020EF001848.

Manoj, J. A., Guntu, R. K. & Agarwal, A. (2022) Spatiotemporal dependence of soil moisture and precipitation over India, *Journal of Hydrology*, **610**, 127898. ISSN 0022-1694. https://doi.org/10.1016/j.jhydrol.2022.127898.

Mishra, V., Thirumalai, K., Singh, D. & Aadhar, S. (2020) Future exacerbation of hot and dry summer monsoon extremes in India, *npj Climate and Atmospheric Science*, **3**, 10. https://doi.org/10.1038/s41612-020-0113-5.

Moftakhari, H. R., Salvadori, G., AghaKouchak, A., Sanders, B. F. & Matthew, R. A. (2017) Compounding effects of sea level rise and fluvial flooding, *Proceedings of the National Academy of Sciences*, **114**, 9785–9790. doi:10.1073/pnas.1620325114.

Mondal, S., Mishra, A. K. & Leung, L. R. (2020) Spatiotemporal characteristics and propagation of summer extreme precipitation events over the United States: a complex network analysis, *Geophysical Research Letters*, **47**, e2020GL088185. https://doi.org/10.1029/2020GL088185.

Odenweller, A. & Donner, R. (2020) Disentangling synchrony from serial dependency in paired-event time series, *Physical Review E*, **101**, 052213. https://doi.org/10.1103/PhysRevE.101.052213.

Pai, D., Sridhar, L., Rajeevan, M., Sreejith, O. P., Satbhai, N. S. & Mukhopadhyay, B. (2014) Development of a new high spatial resolution (0.25° × 0.25°) long period (1901–2010) daily gridded rainfall data set over India and its comparison with existing data sets over the region, *Mausam*, **65**, 1–18. https://doi.org/10.54302/mausam.v65i1.851.

Pendergrass, A. G. (2018) What precipitation is extreme?, *Science*, **360**, 1072–1073. doi:10.1126/science.aat1871.

Perkins, S. E. & Alexander, L. V. (2013) On the measurement of heat waves, *Journal of Climate*, **26** (13), 4500–4517. doi:10.1175/JCLI-D-12-00383.1.

Perkins-Kirkpatrick, S. E. & Lewis, S. C. (2020) Increasing trends in regional heatwaves, *Nature Communications*, **11** (1), 3357. doi:10.1038/s41467-020-16970-7.

Prein, A. F., Rasmussen, R. M., Ikeda, K., Liu, C., Clark, M. P. & Holland, G. J. (2017) The future intensification of hourly precipitation extremes, *Nature Climate Change*, **7** (1), 48–52. https://doi.org/10.1038/nclimate3168.

Rahmstorf, S. & Coumou, D. (2011) Increase of extreme events in a warming world, *Proceedings of the National Academy of Sciences*, **108**, 17905–17909. doi:10.1073/pnas.1101766108.

Regmi, M. B. & Hanaoka, S. (2011) A survey on impacts of climate change on road transport infrastructure and adaptation strategies in Asia, *Environmental Economics and Policy Studies*, **13**, 21–41. doi:10.1007/s10018-010-0002-y.

Rehana, S., Nannaka, V. & Mummidivarapu, S. K. (2024) Variations of compound warm, dry, wet, and cold climate extremes in India during 1951 to 2014, *Science of the Total Environment*, **950**, 175164. https://doi.org/10.1016/j.scitotenv.2024.175164.

Ridder, N. N., Pitman, A. J., Westra, S., Ukkola, A., Do, H. X., Bador, M., Hirsch, A. L., Evans, J. P., Di Luca, A. & Zscheischler, J. (2020) Global hotspots for the occurrence of compound events, *Nature Communications*, **11**, 5956. https://doi.org/10.1038/s41467-020-19639-3.

Sabeerali, C. T., Rao, S. A., Ajayamohan, R. & Murtugudde, R. (2012) On the relationship between Indian summer monsoon withdrawal and Indo-Pacific SST anomalies before and after 1976/1977 climate shift, *Climate Dynamics*, **39**, 841–859. https://doi.org/10.1007/s00382-011-1269-9.

Sahana, A. S., Ghosh, S., Ganguly, A. & Murtugudde, R. (2015) Shift in Indian summer monsoon onset during 1976/1977, *Environmental Research Letters*, **10**, 054006. https://doi.org/10.1088/1748-9326/10/5/054006.

Saidi, H., Ciampittiello, M., Dresti, C. & Ghiglieri, G. (2015) Assessment of trends in extreme precipitation events: a case study in piedmont (North-West Italy), *Water Resources Management*, **29**, 63–80. 10.1007/s11269-014-0826-5.

Salunke, P., Keshri, N., Mishra, S. & Dash, S. (2023) Future projections of seasonal temperature and precipitation for India, *Frontiers in Climate*, **5**, 1069994. 10.3389/fclim.2023.1069994.

Sauter, C., Fowler, H. J., Westra, S., Ali, H., Peleg, N. & White, C. J. (2023) Compound extreme hourly rainfall preconditioned by heatwaves most likely in the mid-latitudes, *Weather and Climate Extremes*, **40**, 100563. https://doi.org/10.1016/j.wace.2023.100563.

Sedlmeier, K., Feldmann, H. & Schädler, G. (2018) Compound summer temperature and precipitation extremes over central Europe, *Theoretical and Applied Climatology*, **131**, 1493–1501. https://doi.org/10.1007/s00704-017-2061-5.

Sheridan, S. C. & Lee, C. C. (2018) Temporal trends in absolute and relative extreme temperature events across North America, *Journal of Geophysical Research: Atmospheres*, **123**, 11889–11898. doi:10.1029/2018JD029150.

Siegmund, J. F., Siegmund, N. & Donner, R. V. (2017) Coincalc – a new R package for quantifying simultaneities of event series, *Computers & Geosciences*, **98**, 64–72. https://doi.org/10.1016/j.cageo.2016.10.004.

Siegmund, J. F., Wiedermann, M., Donges, J. F. & Donner, R. V. (2016) Impact of temperature and precipitation extremes on the flowering dates of four German wildlife shrub species, *Biogeosciences*, **13**, 5541–5555. https://doi.org/10.5194/bg-13-5541-2016.

Stone Jr., B., Mallen, E., Rajput, M., Gronlund, C. J., Broadbent, A. M., Krayenhoff, E. S., Augenbroe, G., O'Neill, M. S. & Georgescu, M. (2021) Compound climate and infrastructure events: how electrical grid failure alters heat wave risk, *Environmental Science & Technology*, **55** (10), 6957–6964. https://doi.org/10.1021/acs.est.1c00024.

Sun, Q., Miao, C., AghaKouchak, A. & Duan, Q. (2017) Unraveling anthropogenic influence on the changing risk of heat waves in China, *Geophysical Research Letters*, **44** (10), 5078–5085. doi:10.1002/2017GL073531.

Taylor, C. M., Belušić, D., Guichard, F., Parker, D. J., Vischel, T., Bock, O., Harris, P. P., Janicot, S., Klein, C. & Panthou, G. (2017) Frequency of extreme Sahelian storms tripled since 1982 in satellite observations, *Nature*, **544**, 475–478. doi:10.1038/nature22069.

Trenberth, K., Dai, A., van der Schrier, G., Jones, P. D., Barichivich, J., Briffa, K. R. & Sheffield, J. (2014) Global warming and changes in drought, *Nature Climate Change*, **4**, 17–22. https://doi.org/10.1038/nclimate2067.

Trenberth, K. E., Dai, A., Rasmussen, R. M. & Parsons, D. B. (2003) The changing character of precipitation, *Bulletin of the American Meteorological Society*, **84** (9), 1205–1218. https://doi.org/10.1175/BAMS-84-9-1205.

Wahl, T., Jain, S., Bender, J., Meyers, S. D. & Luther, M. E. (2015) Increasing risk of compound flooding from storm surge and rainfall for major US cities, *Nature Climate Change*, **5**, 1093–1097. 10.1038/nclimate2736.

Wu, H., Su, X. & Singh, V. P. (2023) Increasing risks of future compound climate extremes with warming over global land masses, *Earth's Future*, **11**, e2022EF003466. https://doi.org/10.1029/2022EF003466.

You, J., Wang, S., Zhang, B., Raymond, C. & Matthews, T. (2023) Growing threats from swings between hot and wet extremes in a warmer world, *Geophysical Research Letters*, **50** (14), e2023GL104075. https://doi.org/10.1029/2023GL104075.

Zhai, P., Zhang, X., Wan, H. & Pan, X. (2005) Trends in total precipitation and frequency of daily precipitation extremes over China, *Journal of Climate*, **18** (7), 1096–1108. doi:10.1175/JCLI-3318.1.

Zscheischler, J., Martius, O., Westra, S., Bevacqua, E., Raymond, C., Horton, R. M., van den Hurk, B., AghaKouchak, A., Jézéquel, A., Mahecha, M. D., Maraun, D., Ramos, A. M., Ridder, N. N., Thiery, W. & Vignotto, E. (2020) A typology of compound weather and climate events, *Nature Reviews Earth & Environment*, **1**, 333–347. doi:10.1038/s43017-020-0060-z.

Zscheischler, J., Westra, S., Van Den Hurk, B. J. J. M., Seneviratne, S. I., Ward, P. J., Pitman, A., AghaKouchak, A., Bresch, D. N., Leonard, M., Wahl, T. & Zhang, X. (2018) Future climate risk from compound events, *Nature Climate Change*, **8**, 469–477. doi:10.1038/s41558-018-0156-3.

First received 2 September 2025; accepted in revised form 23 February 2026. Available online 24 March 2026